Journal of Power Sources 196 (2011) 6400–6411

Contents lists available at ScienceDirect

Journal of Power Sources

journal homepage: www.elsevier.com/locate/jpowsour

Synthesis, characterization and application of $Li_3Fe_2(PO_4)_3$ nanoparticles as cathode of lithium-ion rechargeable batteries

Hassan Karami*, Foroozandeh Taala

Nano Research Laboratory, Chemistry Department, Payame Noor University, Abhar, Iran

ARTICLE INFO

Article history:
Received 20 January 2011
Received in revised form 24 March 2011
Accepted 27 March 2011
Available online 5 April 2011

Keywords:
Lithium iron phosphate
Gel combustion
Nanoparticles
Cathode material
Cyclic voltammetry
Lithium-ion batteries

ABSTRACT

This work introduces a new method to synthesize $Li_3Fe_2(PO_4)_3$ nanoparticles in the nanopowder form and study its electrochemical performance by cyclic voltammetry and battery tests. $Li_3Fe_2(PO_4)_3$ is synthesized by the gel combustion method based on polyvinyl alcohol (PVA) as gel making agent. The optimum conditions of the synthesis include 8 wt% PVA, 0.34 wt% lithium slat, 1 wt% iron salt, 0.57 wt% ammonium dihydrogen phosphate, ethanol–water 50:50 as solvent, 675 °C combustion temperature and 4 h combustion time. Characterization of the samples is performed by the scanning electron microscopy (SEM), transmission electron microscopy (TEM), EDX analysis, XRD patterns, BET specific surface area and DSL size distribution. In the optimum conditions, a nanopowder is obtained that consisting of uniform nanoparticles with an average diameter of 70 nm. The optimized sample shows 12.5 $m^2 g^{-1}$ specific surface areas. Cyclic voltammetry (CV) studies show that the synthesized compound has good reversibility and high cyclic stability. The CV results are confirmed by the battery tests. The obtained results show that the synthesized cathodic material has high practical discharge capacity (average 125.5 mAh g^{-1} approximately same with its theoretical capacity 128.2 mA h^{-1}) and long cycle life.

1. Introduction

Lithium ion secondary batteries have been widely utilized as energy sources in many electronic devices such as: laptop computers, mobile phones, cellular phones, wireless devices, camcorders, digital cameras and electric vehicles [1–3]. Various compounds such as $Li_xNi_yO_z$ [4–10], $Li_xCo_yO_z$ [9–17], $Li_xMn_yO_z$ [18–25] and $Li_xFe_y(PO_4)_z$ [26–37] have been used as positive materials of Li-ion batteries.

Lithium iron phosphates are new cathodic materials of Li-ion batteries. Among the iron compounds, $Li_3Fe_2(PO_4)_3$ (2.8 V vs. Li^+/Li) [26], $LiFePO_4$ (3.45 V vs. Li^+/Li) [27] and $Fe_2(SO_4)_3$ (3.6 V vs. Li^+/Li) [28], can be used as positive poles vs. lithium anode. Comparing $LiFePO_4$ and $Li_3Fe_2(PO4)_3$ as positive materials shows that all of them have been used successfully as cathode of Li-ion batteries commercially. These materials demonstrated good reversibility for the Fe^{3+}/Fe^{2+} couple redox. Iron compounds have the advantages of low cost, excellent thermal stability, satisfactory safety, low toxicity and natural abundance. Meanwhile lithium iron phosphates have received much attention as an interesting cathode material for Li-ion batteries. Lithium iron phosphate has two abundant forms $LiFePO_4$ and $Li_3Fe_2(PO_4)_3$. In $LiFePO_4$, iron ion is in oxidation state of 2+ and in $Li_3Fe_2(PO4)_3$, it has oxidation state of 3+. Olivine-type $LiFePO_4$ and Nasicon-type $Li_3Fe_2(PO_4)_3$ were proposed to be new candidates for the positive electrode materials. Nasicon-type $Li_3Fe_2(PO_4)_3$ has theoretical capacity (128.2 mAh g^{-1}) lower than the Olivine $LiFePO_4$ (theoretical capacity of 170 mAh g^{-1}) [28–30] but, Nasicon-type has some advantages as following:

1. Nasicon-type has relatively good ionic conductivity resulting from the disorder of lithium ions in the structure [28,37–44], against $LiFePO_4$ [27,35,45–49].
2. It is more stable than Olivne-type.
3. The synthesis of $Li_3Fe_2(PO_4)_3$ is easier than $LiFePO_4$ [50].
4. As result of Fe^{3+}/Fe^{2+} couple redox, 2 mol Li^+ can be intercalated into 1 mol $Li_3Fe_2(PO_4)_3$ reversibly [28,42].

On the other hand, despite extensive investigations in fabrication and characterization on $LiFePO_4$ this material has not currently been used as a commercial cathode material in Li-ion batteries because:

1. The synthesis of $LiFePO_4$ is not easy because of the iron oxidation state the undesired impurity phases, such as Fe_2O_3 and $Li_3Fe_2(PO_4)_3$, existed in the final $LiFePO_4$ products are inevitable [50].
2. Its poor rate capability, which is attributed to the low electronic conductivity and slow kinetics of lithium ion diffusion through the $LiFePO_4$–$FePO_4$ interfaces [46,51].

* Corresponding author. Tel.: +98 912 390 8218; fax: +98 242 522 6932.
E-mail address: karami_h@yahoo.com (H. Karami).

0378-7753/$ – see front matter © 2011 Elsevier B.V. All rights reserved.
doi:10.1016/j.jpowsour.2011.03.079

Based on the above-mentioned advantages of $Li_3Fe_2(PO_4)_3$ and disadvantages of $LiFePO_4$, the Nasicon-type $Li_3Fe_2(PO_4)_3$ can be selected as better cathodic material for more studies.

$Li_3Fe_2(PO_4)_3$ has two crystalline modifications, β-$Fe_2(SO_4)_3$-type crystal structure and Nasicon-type structure [27,28,38–40,52]. For the Nasicon-type compounds $A_3Fe_2(XO_4)_3$ (A = Li, Na; X = P, As, S), its 3D framework is made up of XO_4 tetrahedra and the FeO_6 octahedra. Each FeO_6 octahedron shares its corners with six tetrahedral and each XO_4 tetrahedron is connected by four FeO_6 octahedra. This structure allows lithium intercalation and extraction, making it a promising cathode material for lithium batteries [29]. $Li_3Fe_2(PO_4)_3$ has three phases reported [38] namely, low temperature monoclinic ($P2_1/n$) α, low temperature monoclinic ($P2_1/n$) β and high temperature rhombohedral ($R3c$) γ [53].

Also two immaculateness of Nasicon-type $Li_3Fe_2(PO_4)_3$ has recently received much attention. One is that it has unusual transport behavior and another is its application as solid electrolytes for incorporation into electrochemical devices. In 2008, Nagamine et al. reported that glass–ceramics containing $Li_3Fe_2(PO_4)_3$ phase have been prepared and could be used in the lithium-ion batteries as solid electrolyte [43]. In 1998, the first time Masquelier et al. [28] reported reversible intercalation of lithium into $Li_{3+x}Fe_2(PO_4)_3$ with up to two atoms per formula unit associated with electrochemical reduction of Fe^{3+} to Fe^{2+}. Therefore $Li_3Fe_2(PO_4)_3$ may also be used as a cathode material in rechargeable lithium batteries [29]. The charge/discharge reactions for $Li_3Fe_2(PO_4)_3$ in Li-ion batteries are as follows [44]:

$$\text{Dischargestep}: \quad 2Li^+ + Li_3Fe_2(PO_4)_3 + 2e \rightarrow Li_5Fe_2(PO_4)_3$$

$$\text{Chargestep}: \quad Li_5Fe_2(PO_4)_3 \rightarrow Li_3Fe_2(PO_4)_3 + 2Li^+ + 2e$$

During charge/discharge processes, an intermediate phase $Li_4Fe_2(PO_4)_3$ exist between $Li_3Fe_2(PO_4)_3$ and $Li_5Fe_2(PO_4)_3$ phases[44].

It is obvious that use of nanostructured $Li_3Fe_2(PO_4)_3$ can increase its discharge capacity and some other battery performance parameters. $Li_3Fe_2(PO_4)_3$ nanostructures have been commonly synthesized via hydrothermal methods [52,54], solid-state reactions [2,28,42], ultrasonic spray combustion [40], ion-exchanging (aqueous solution) [28,41], sol–gel route [55,56], melt-quenching method [55] and glass–ceramic processing [43,57]. Based on our best acknowledge, there is not any report about synthesis of $Li_3Fe_2(PO_4)_3$ by the gel combustion method.

In this work, a new synthesis method, using an alcoholic colloidal suspension, was developed by a sequence of systematic chemical reactions. We focused our attention on the synthesis of $Li_3Fe_2(PO_4)_3$ by a new sol–gel combustion method based on polyvinyl alcohol as gel making agent to synthesis uniform nanostructures. The advantages of the synthesis method has been used in this work are low cost of raw material, simple process, short synthesis time. The presented method can be used to produce the nanomaterials in small and large amounts. The synthesized compound was used as working electrode material in cyclic voltammetry (CV) and cathode material in lithium-ion batteries. The obtained results by CV and battery tests showed that the sample has good reversibility, excellent discharge capacity and long cycle life.

2. Experimental

2.1. Materials and reagents

All reagents and compounds were in the analytical grade and obtained from Merck, Fluka and Loba Chimie (India). Double-distilled water was used in all experiments.

2.2. Instrumentals

The morphology of the samples was characterized by scanning electron microscopy (MODLE-(XL-30) PHILIPS HOLLAND). Transmission electron microscope (Zeiss EM900, 80 keV) was used for exactly determining size and shape of particles. The composition and particle sizes of the samples were determined by XRD (E" Pert-MPD Phillips, Netherland). The particle sizes and effective surface area were determined by BET measurements based on N_2 adsorption/desorption isothermal diagrams (Temcem 902 A Z Picc, Germany). Size distribution diagram of the optimized sample was obtained by DLS (Malvern, Zetasizer Nano ZS3600). Cyclic voltammetry studies were performed by Autolab (PGStat 102, EchoChemie). All battery tests were done by full automated battery tester (BTE 06, Iran).

2.3. Procedures

2.3.1. Synthesis procedure

Firstly, 0.57 g ammonium dihydrogen phosphate was dissolved in 90.03 g ethanol–water (50:50). 0.34 g lithium nitrate and 1.06 g iron (III) nitrate were added to the obtained solution and then, 8 g PVA was dissolved to form a low viscose solution which called "Sol". During sol formation, solution temperature was kept lower than 80 °C. After sol formation, the mixture was slowly heated to form a homogeneous gel. The obtained gel was heated to completely evaporate its solvent until it forms a dried gel under H_2/N_2 (10/90) atmosphere. The obtained gel was pyrrolized at 675 °C for 4 h under H_2/N_2 (10/90) atmosphere. At this stage, H_2/N_2 atmosphere prevents the forming of Fe_2P, decreases Fe_2O_3 and increases yield of $Li_3Fe_2(PO_4)_3$.

2.3.2. Cyclic voltammetry procedure

The optimized $Li_3Fe_2(PO_4)_3$ sample was mixed with 10 wt% PTFE and 10 wt% Acetylene black in N-methylpyrrolidinone to form slurry. The slurry was spread uniformly on a thin aluminum foil with a diameter of 10 mm, and then were vacuum dried for 3 h at 120 °C. The obtained disks were used as working electrodes in electrochemical studies. Cyclic voltammetric behaviors of the prepared electrodes as working electrodes were investigated in the potential window of 2–4 V vs. two 1 cm × 1 cm metallic lithium plates as counter and reference electrodes in 1 M $LiPF_6$ solution in 1:1 EC and DMC mixed solvent under Argon atmosphere. Reversibility of $Li_3Fe_2(PO_4)_3$ as electroactive material was investigated during 50 cycles with potential scan rate of 0.1 mV s^{-1}.

2.3.3. Battery construction and tests

For battery construction, some battery devices were designed as Fig. 1. In the device, more amount of metallic lithium with respect to $Li_3Fe_2(PO_4)_3$ value was put down by 2 atmosphere pressure into the anodic hole. $Li_3Fe_2(PO_4)_3$ powder was mixed with 10 wt% PTFE and 10 wt% Acetylene black in N-methylpyrrolidinone to form slurry (the same with working electrode in CV). The slurry was heated to concentrate and to obtain a uniform paste. The paste was filled into cathodic hole in the battery device. After pasting the cathodic part, the pastet part was vacuum dried for 3 h at 120 °C. Each dried cathode contained 80 mg $Li_3Fe_2(PO_4)_3$ nanopowder with purity of 75 wt% that was laminated on the floor of cathodic hole with 10 mm diameter and 1 mm thickness. The dried cathodic part was saturated with battery electrolyte (1 M $LiPF_6$ solution in 1:1 EC and DMC mixed solvent). One layer polyamide separator was laminated between cathode and anode parts, then two battery parts were screwed together as it was shown in Fig. 1b.

The screwed batteries were charged with 10 mA constant current for 1 h to obtain fully charged batteries. Then, the fully charged batteries were discharged by 10 mA constant current to decrease

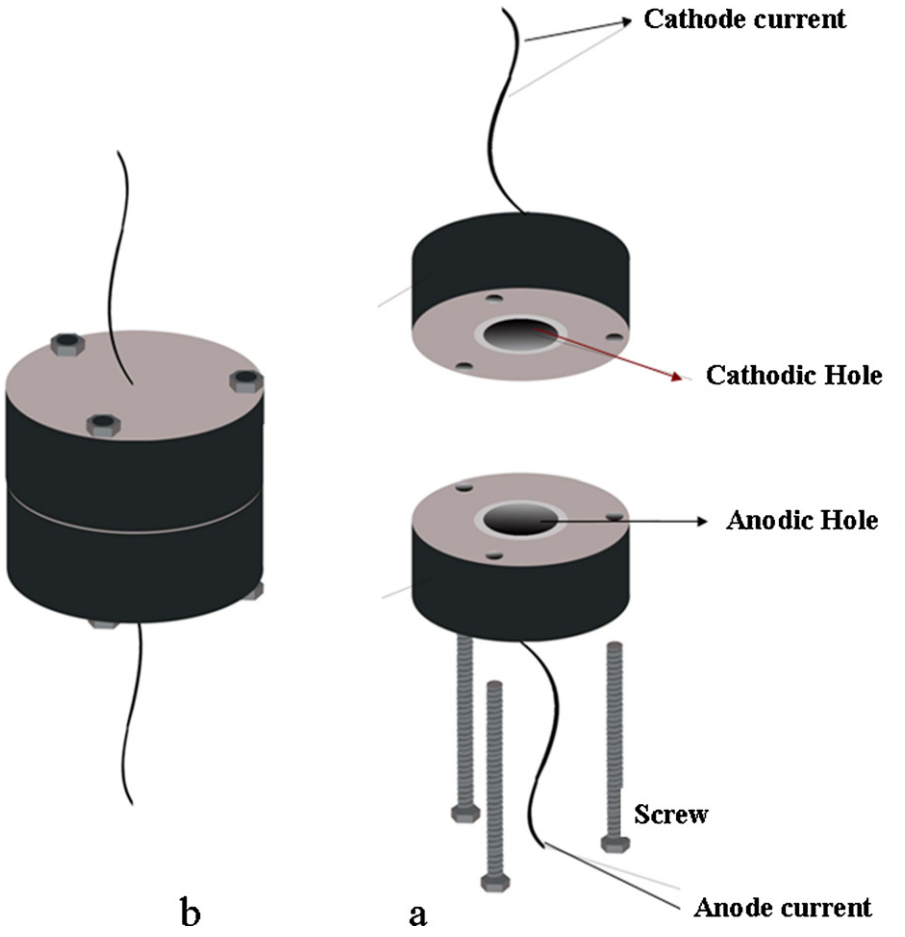

Fig. 1. Scheme of the parts of the used battery (a) and the final screwed battery (b).

the battery voltage to 2.3 V. In the cycle life test, the charge process was done by 10 mA constant current for 1 h and then, the battery was kept in rest for 1 min. Finally, the battery was discharged by 10 mA constant current to cut off voltage of 2.3 V. A charge, a rest and a consecutive discharge step is regarded as one cycle life. The three step cycle was repeated for 75 times.

3. Results and discussion

3.1. Synthesis

In the gel combustion method, the gel network rigidity controls the morphology and particle size of the synthesized sample to make a uniform nanostructured $Li_3Fe_2(PO_4)_3$. In the gel structure, all salts were homogeneously dispersed among polymeric network [58]. Because of gel network rigidity, the dispersed ions in the gel network cannot alter their positions. Therefore, during the combustion of the gel's outer layers, lithium, iron and phosphate ions of the burnt layers combine with each other to create the $Li_3Fe_2(PO_4)_3$ nanoparticles.

The polyvinyl alcohol (PVA), generally used as suspension stabilizer, exhibits the effect of reducing particle size of the polymer by decreasing the surface tension and by improving the dispersion of the reactants during the polymerization reaction. The polyvinyl alcohol (PVA) is a hydrophilic polymer contributing hydroxyl group on each of its repeating units, which permits the development of hydrogen bonds with the hydroxyl and carboxyl groups of reactants. The PVA prolongs sedimentation reaction therefore particles trammel in gel pores while the solvent gently evaporates, thus there is no repeated impact. In this method, the amount of PVA, $Fe(NO_3)_3$, $LiNO_3$, $NH_4H_2PO_4$, PVA, the mixed solvent composition, temperature and time of combustion can change the composition, morphology, and particle size of the sample. The degree of these effects was optimized by the "one at a time" method.

3.1.1. Optimization of solvent composition

First, six samples were synthesized at different ratios of ethanol/water. Figs. 2 and 3 show the SEM images of the synthesized samples of these experiments with 10,000× and 20,000× magnifications, respectively. The used salts and PVA are insoluble in pure ethanol (without water) but it is soluble in pure water (without ethanol). To obtain a uniform nanostructure, having a uniform and rigid gel is necessary. Based on the obtained results, the mixed solvent with composition of 50:50 ethanol/water has suitable polarity to dissolve all salts and PVA which can be used to form a homogeneous gel. For more clarification of solvent effect on the particle sizes, average particle sizes of all samples were calculated from SEM data. Fig. 4 shows the effect of solvent composition (as ethanol concentration in water) on the average size of the particles. Based on these results, ethanol/water with 1:1 ratio is suitable to obtain a uniform solution and the smallest nanoparticles. For evaluation of solvent effect, polarity index (Snider index) was calculated for all solvent (Table 1). As it can be seen in Table 1, the mixed solvent (ethanol:water 50:50) has suitable polarity to dissolve all components (lithium salt, iron salt, ammonium dihydrogen phosphate and PVA). Therefore, in this polarity, the most homogenized gel can be obtained to produce the smallest and most uniform particles.

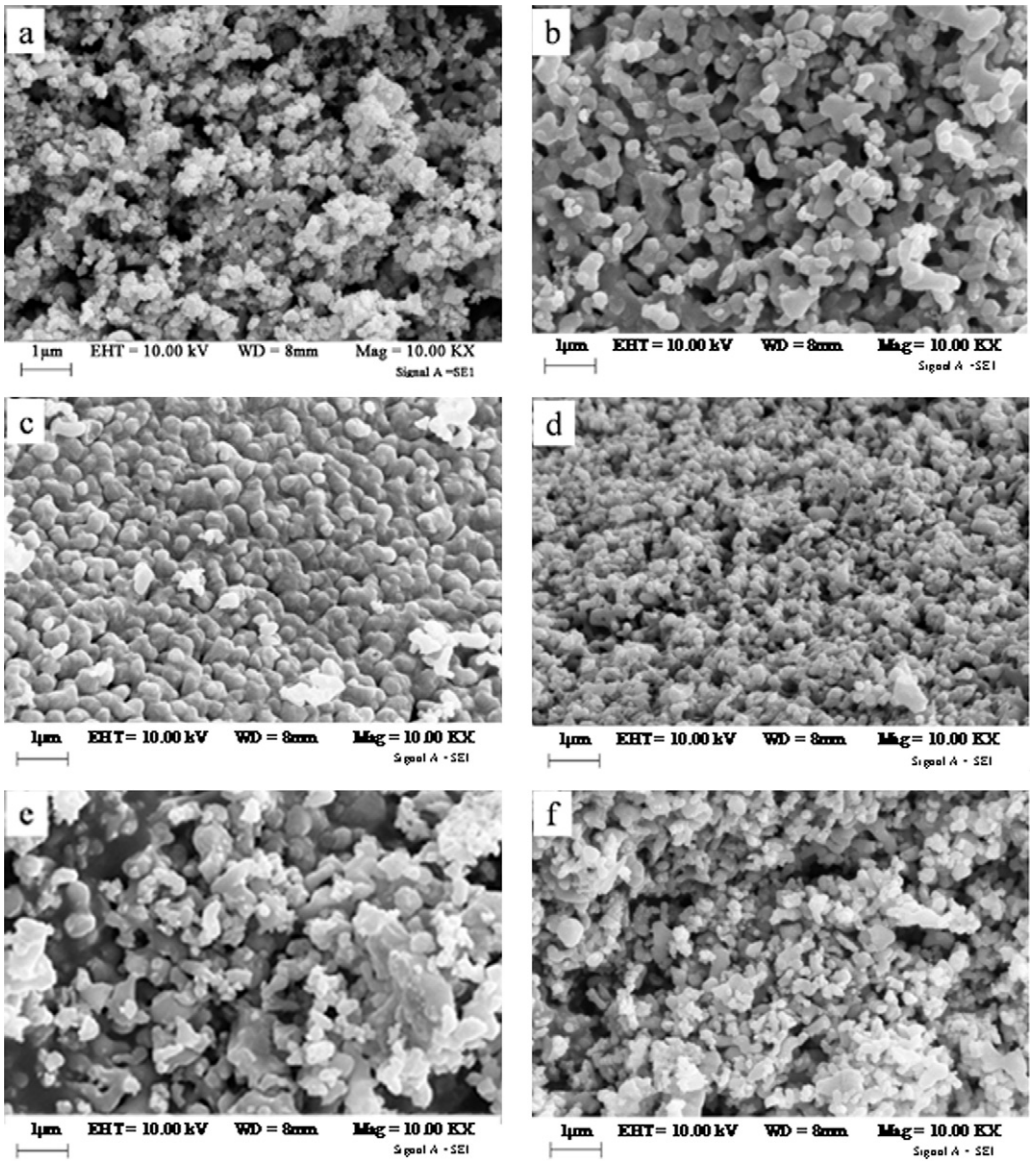

Fig. 2. Effect of solvent composition on the SEM images of the samples synthesized at ethanol: water ratios of (a) 15:85, (b) 25:75, (c) 37.5:62.5, (d) 50:50, (e) 62.5:37.5 and (f) 75:25 with 10,000× magnification.

Table 1
Effect of solvent polarity on the particle sizes.

Solvent (ethanol:water)	15:85	25:75	37.5:62.5	50:50	62.5:37.5	75:25
Polarity index	9.3	8.7	8.0	7.2	6.5	5.7
Average particle sizes	250	335	296	142	337	304

3.1.2. Optimization of PVA content

Six synthesizes were performed at different amounts of PVA while the amounts of other parameters were kept constant. Fig. 5 shows the effect of PVA content on the morphology and particle size of $Li_3Fe_2(PO_4)_3$ nanoparticles. The initial amount of PVA in the sol is an important agent to make a uniform three dimensional gel. During gel making process, the used salts (lithium nitrate, iron nitrate and ammonium phosphate) were distributed throughout the gel network. Based on the PVA content, the gel network has a limited capacity to entire inorganic salts into holes. Therefore, the weight ratio of PVA to salts in the initial sol is an important parameter to control particle growth mechanism. As it can be seen from Fig. 5, 8 wt% PVA is an optimum value for $Li_3Fe_2(PO_4)_3$ synthesis. At this amount, gel network structure is suitable for controlling $Li_3Fe_2(PO_4)_3$ synthesis to obtain uniform nanoparticles with 80 nm average diameter.

3.1.3. Salts effects

Various samples were synthesized at different values of lithium nitrate, iron nitrate and ammonium dihydrogen phosphate. Initial studies show the ratio of 2:1:2 for these salts is suitable to synthesis $Li_3Fe_2(PO_4)_3$ with more purity. Fig. 6 shows the SEM images of 5 samples were synthesized at different amounts of three salts. As it is obvious in Fig. 6, at the ratio of 2:1:2, 1.06 wt% iron nitrate, 0.34 wt% lithium nitrate and 0.57 wt% ammonium dihydrogen phosphate is suitable to synthesize smaller and uniform particles of $Li_3Fe_2(PO_4)_3$. Therefore, these amounts were selected as optimum amounts for future studies. Increasing or decreasing of initial salt amounts has similar effect with PVA content. Rigidity and homogeneity of the gel are changes when the contents of PVA or salts are varied.

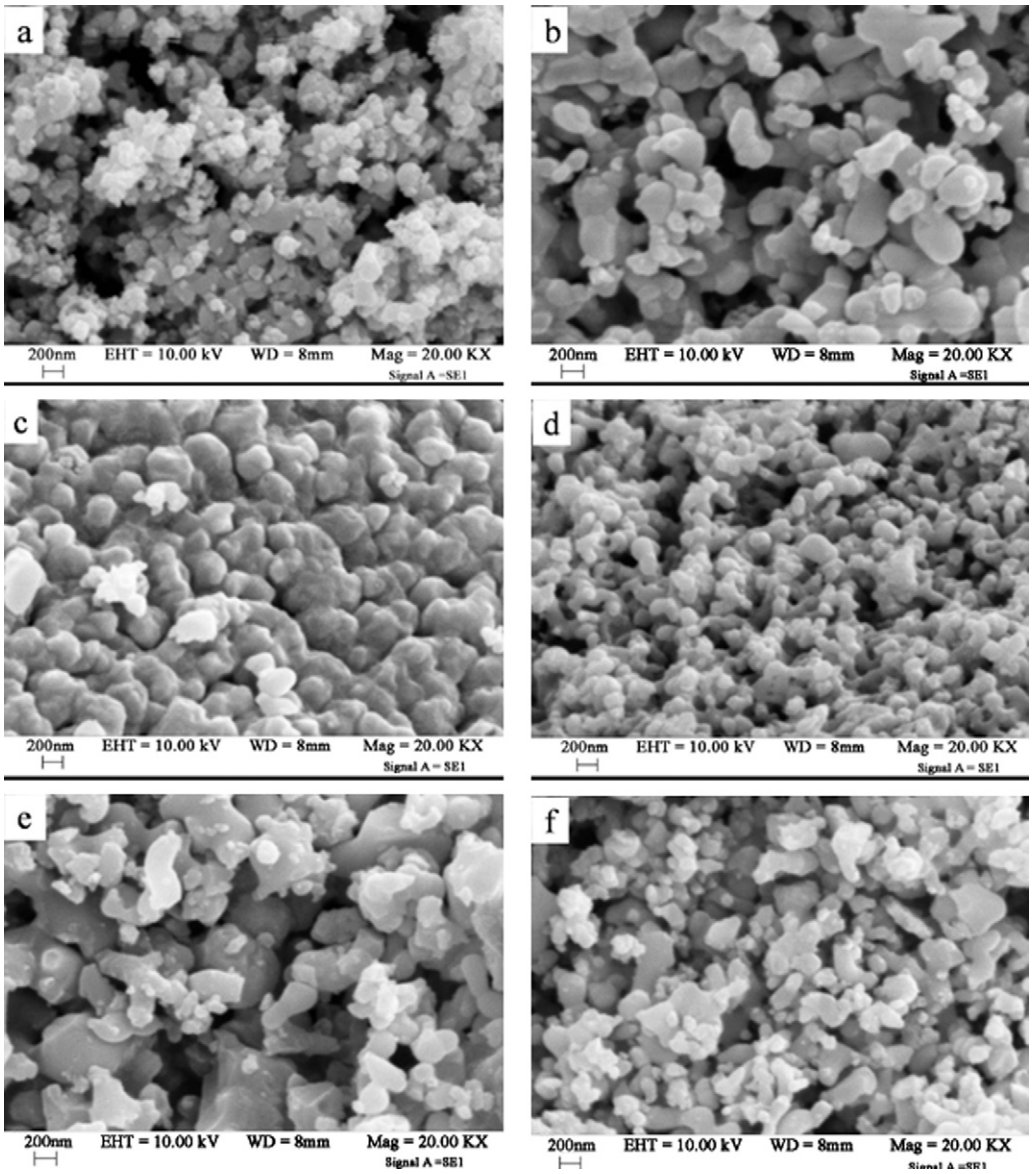

Fig. 3. Effect of solvent composition on the SEM images of the samples synthesized at ethanol: water ratios of (a) 15:85, (b) 25:75, (c) 37.5:62.5, (d) 50:50, (e) 62.5:37.5 and (f) 75:25 with 20,000× magnification.

3.1.4. Optimization of combustion temperature

Among the effective parameters, combustion temperature is a more important parameter that can affect the morphology, particle size and also on the phase composition of the samples. Four samples were synthesized with different temperatures of 475 °C, 575 °C, 675 °C and 775 °C. Fig. 7 shows the SEM images of these samples. As it can be seen in Fig. 7, by decreasing the combustion temperature, the morphology and particle size of samples become more homogenized, including the sampler. The rate of gel combustion is decreased when the furnace temperature is decreased. At lower temperatures, the gel can efficiently controls nucleation and particle growth.

The effect of combustion temperature on the phase composition of samples was studied by XRD patterns (Fig. 8). In Fig. 8, important lines of $Li_3Fe_2(PO_4)_3$ were indexed. Small non-indexed lines were the result of impurities. Based on XRD analysis, all samples have small amounts of impurities such as Fe_2P and Fe_2O_3. At 675 °C, samples with higher purities can be synthesized. Nevertheless, at this temperature, the sample also has small amounts of Fe_2P, Li_3PO_4 and Fe_2O_3 as impurities.

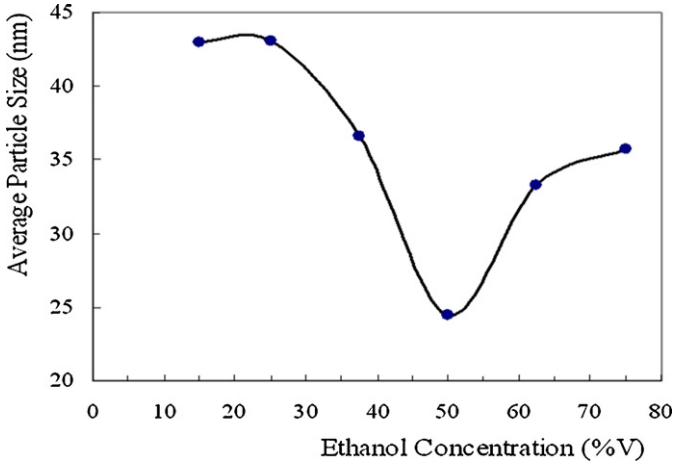

Fig. 4. Effect of solvent composition (as ethanol concentration in water) on the average particle sizes of final yield.

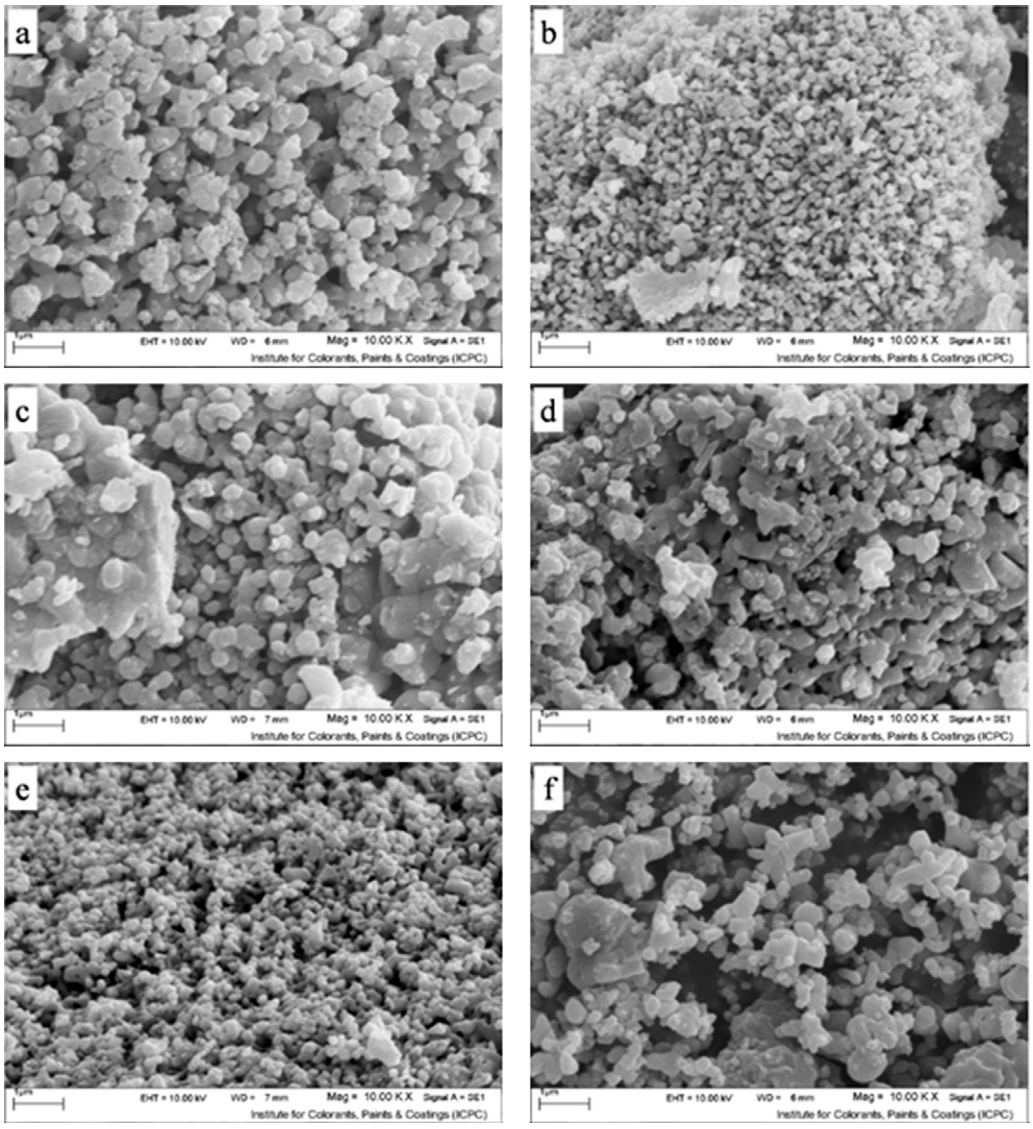

Fig. 5. SEM images of different nanoparticles synthesized at different amounts of PVA; 0 (a), 3 (b), 4.5 (c), 6 (d), 8 (e) and 10 g (f).

Table 2
Calculated particle sizes based on XRD patterns by using Debye–Scherer equation.

Combustion temperature (°C)	2θ (deg)					Average particle size (nm)
	16.5	21	24	27.5	29.5	
475	24.28	24.28	12.73	33.38	12.73	21.48
575	24.28	24.28	14.05	33.38	24.28	24.05
675	24.28	24.28	14.05	24.28	24.28	22.23
775	20.54	20.54	11.13	24.28	20.54	19.41

Particle sizes of the samples were calculated based on Debye–Scherer equation by using XRD peaks (Table 2). As it can be seen in Table 2, combustion temperature does not have a considerable effect on the particle size of the samples. Comparing XRD results by SEM images (Fig. 7) shows an obvious difference. Based on SEM images, particles sizes are increased when the combustion temperature increases but, based on XRD results (Debye–Scherer calculations); combustion temperature does not have a considerable effect on the particle size. When particle boundaries become very thin, SEM cannot resolute these boundaries. Therefore, at a compact sample with small boundaries, many connected particles seem to be one particle.

3.1.5. Atmosphere effect

For reducing impurities, one sample was synthesized in nitrogen atmosphere. Fig. 9 shows the XRD patterns of this sample. Based on XRD patterns, the sample includes Fe_2O_3 and Li_3PO_4 (total weight 24 wt%) and 5 wt% Fe_2P as impurities. The obtained results showed that the presence of inert atmosphere without reducing agent (such as H_2) cannot decrease the amount of impurities. Based on previous reports, the amount of Fe_2P at lithium iron phosphate samples can be reduced by using H_2 atmosphere. Fig. 10 shows the XRD patterns for the sample which synthesized in the H_2/N_2 (10/90) atmosphere. Comparing Fig. 10 with Fig. 9 (and also with Fig. 8) shows that the content of Fe_2P impurity has been eliminated and the contents of Fe_2O_3 andLi_3PO_4 impurity have been reduced.

3.1.6. Characterization of optimized sample

Table 3 shows the experimental results that are suitable to synthesize the smallest and most uniform nanoparticles of $Li_3Fe_2(PO_4)_3$.

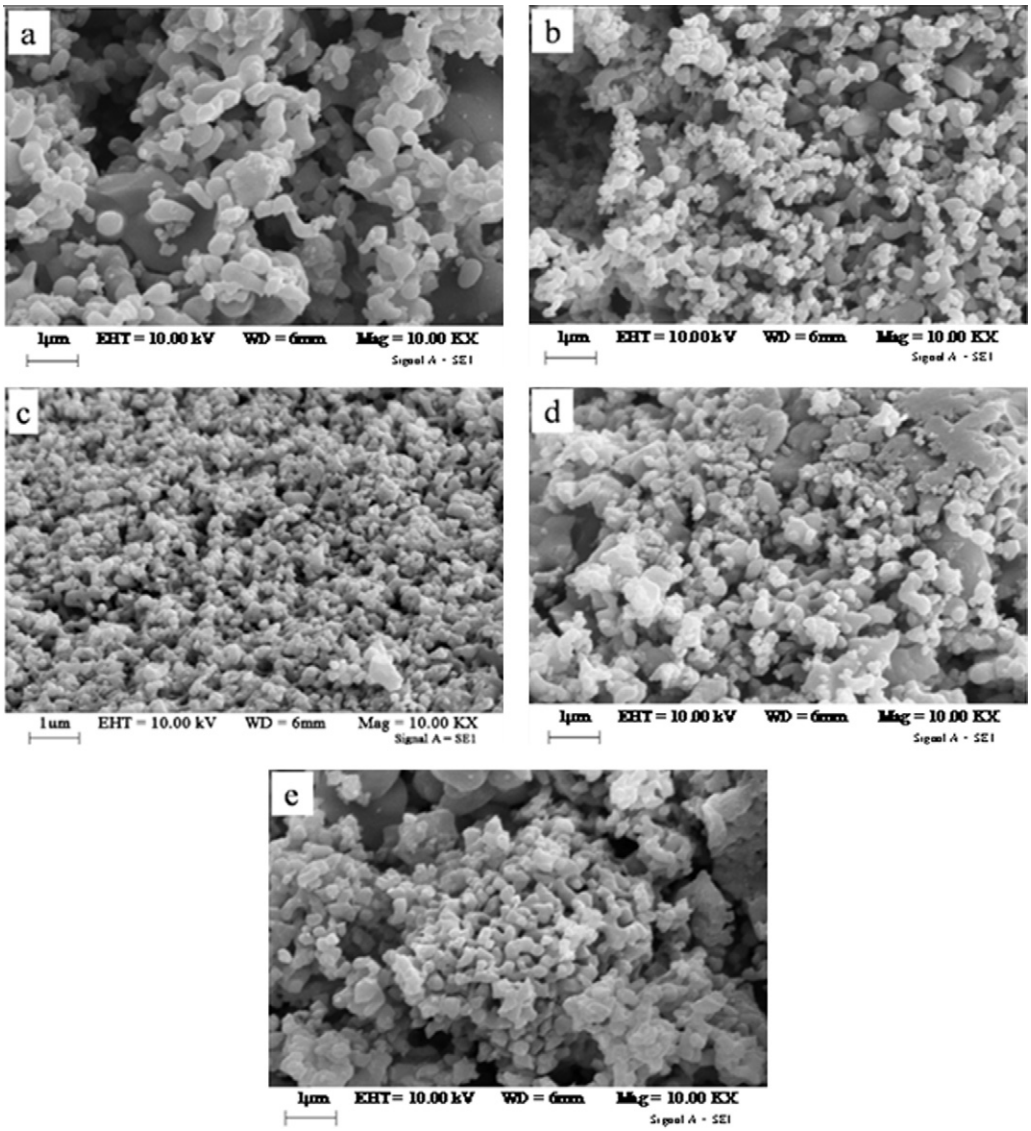

Fig. 6. SEM images of samples synthesized at different levels of initial salts; (a) 0.66 wt% iron nitrate, 0.11 wt% lithium nitrate and 0.19 wt% ammonium dihydrogen phosphate, (b) 1 wt% iron nitrate, 0.17 wt% lithium nitrate and 0.28 wt% ammonium dihydrogen phosphate, (c) 2 wt% iron nitrate, 0.34 wt% lithium nitrate and 0.57 wt% ammonium dihydrogen phosphate, (d) 4 wt% iron nitrate, 0.68 wt% lithium nitrate and 1.14 wt% ammonium dihydrogen phosphate and (e) 6 wt% iron nitrate, 1.02 wt% lithium nitrate and 1.71 wt% ammonium dihydrogen phosphate.

Table 3
Experimental conditions of Nasicon-type $Li_3Fe_2(PO_4)_3$ synthesis.

Parameter	Optimum condition
Solvent composition (ethanol:water)	50:50
PVA (wt%)	8
Salts ratio (lithium nitrate:iron nitrate:ammonium phosphate)	2:1:2
Lithium nitrate (wt%)	0.34
Iron nitrate (wt%)	1.06
Ammonium phosphate (wt%)	0.57
Combustion temperature (°C)	675
Synthesis atmosphere: H_2/N_2	10%V H_2 and 90%V N_2

Fig. 11 shows the SEM image, TEM image and size distribution diagram (DSL) for the optimized sample. As it can be seen in Fig. 10, the sample includes uniform nanoparticles with average 70 nm in diameter.

The specific surface area (SB ($m^2\,g^{-1}$)) was derived from BET-plots of volume adsorbed (V_a ($cm^3(STP)\,g^{-1}$)) vs. the relative pressure ($p/po = 0.25$) as described by Gregg and Sing [59], whereas the cumulative surface area (SC ($m^2\,g^{-1}$)) was obtained by summation of the surface area of pores between 20 and 50 nm radius as determined by means of the mathematical apparatus of the BJH-method [60]. Based on these results, the optimized sample has 12.5 $m^2\,g^{-1}$ specific surface areas. The results reveal that the optimized $Li_3Fe_2(PO_4)_3$ nanoparticles have large specific surface area so that it is expected this material can be used as high performance electroactive materials of lithium-ion batteries.

3.2. Cyclic voltammetry studies

Aluminum based pasted electrode was used as working electrode and coupled with one pair Li electrode in solution containing 1 M $LiPF_6$ in 1:1 EC and DMC mixed solvent under Argon atmosphere. Fig. 12 shows consecutive 50 cyclic voltammograms (CV) for $Li_3Fe_2(PO_4)_3$ nanoparticles where taken in 0.1 mV s^{-1}. As it is seen in Fig. 12, the synthesized compound showed good reversible two peak pairs, consisting of two anodic and two cathodic peaks,

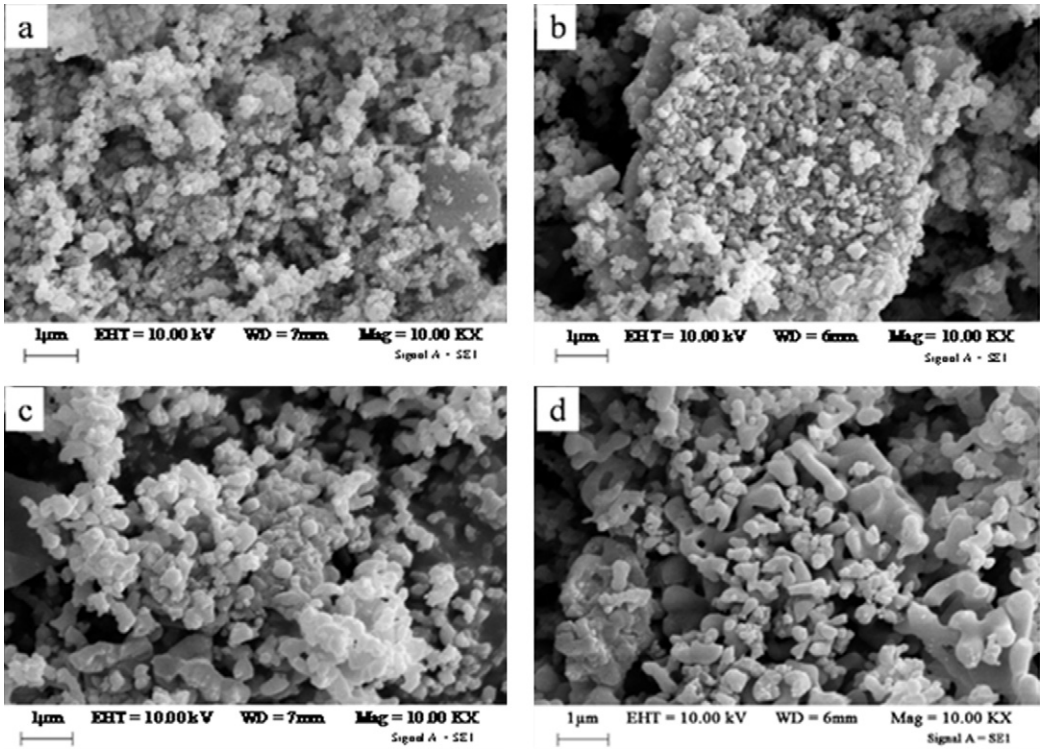

Fig. 7. SEM images of samples synthesized at different temperatures of pyrrolysis; (a) 475 °C, (b) 575 °C, (c) 675 °C and (d) 775 °C.

which correspond to the insertion of two Li^+ for Fe^{3+}/Fe^{2+} redox couple at 2.65 and 2.83 V vs. Li^+/Li. Each redox peak pair has voltage separation of about 50 mV. The first redox peak pair is separated from the second redox peak pair by 180 mV. These results confirm the previous reports [28,41]. Patoux et al. [61] reported $Li_3Fe_2(PO_4)_3$, which is only active for lithium insertion, can reversibly exchange two electrons at ~2.75 V vs. Li/Li (~350 Wh kg^{-1}) onto two distinct plateaus, both corresponding to the reduction of the Fe^{3+} ions into Fe^{2+} for $Li_5Fe_2(PO_4)_3$. The observed peaks are related to the following reactions:

$$\text{Firstreductionpeak}(2.60\,\text{Vvs.Li}^+): \quad \text{Li}^+ + \text{Li}_3\text{Fe}_2(\text{PO}_4)_3 + e \rightarrow \text{Li}_4\text{Fe}_2(\text{PO}_4)_3$$

$$\text{Firstoxidationpeak}(2.70\,\text{Vvs.Li}^+/\text{Li}): \quad \text{Li}_4\text{Fe}_2(\text{PO}_4)_3 \rightarrow \text{Li}^+ + \text{Li}_3\text{Fe}_2(\text{PO}_4)_3 + e$$

$$\text{Secondreductionpeak}(2.78\,\text{Vvs.Li}^+): \quad \text{Li}^+ + \text{Li}_4\text{Fe}_2(\text{PO}_4)_3 + e \rightarrow \text{Li}_5\text{Fe}_2(\text{PO}_4)_3$$

$$\text{Secondoxidationpeak}(2.88\,\text{Vvs.Li}^+): \quad \text{Li}_5\text{Fe}_2(\text{PO}_4)_3 \rightarrow \text{Li}^+ + \text{Li}_4\text{Fe}_2(\text{PO}_4)_3 + e$$

During 50 cycles, the heights of all peaks were increased. Based on the XRD results (Figs. 8–10), the initial samples have Fe_2O_3 and Li_3PO_4 as impurities. These impurities of the synthesized sample can be slowly converted into the $Li_3Fe_2(PO_4)_3$ during 50 cycles. Therefore, during 50 cycles, the amount of $Li_3Fe_2(PO_4)_3$ will be increased so that, the heights of four redox peaks will be increased. XRD patterns of the sample used in CV studies before and after CV experiments (50 cycles) confirmed that major amounts of Fe_2O_3 and Li_3PO_4 (as synthesis impurities) can be converted into $Li_3Fe_2(PO_4)_3$ during 50 cycles (Fig. 13). Based on the obtained results from XRD patterns, the total amount of impurities (Fe_2O_3 and Li_3PO_4) decreased from 24 wt% before CV experiments to 5 wt% after CV experiments (after 50 cycles). It should be mentioned that paste of working electrode in CV experiments includes 90 wt% $Li_3Fe_2(PO_4)_3$ powder, 10 wt% PTFE and 10 wt% Acetylene black (see Section 2.3.2), so XRD patterns for this mixture is very complex. For more clarification, all peaks of additives were subtracted by the XRD soft ware.

The reaction of cyclic voltammetry is exactly similar to the reactions of the lithium-ion batteries. There, it can be expected that the discharge capacity of the synthesized sample in lithium-ion battery will be increased during some initial charge/discharge cycles.

3.3. Battery construction and tests

During synthesis optimization, the morphology and particles sizes were considered as optimizing parameters. The optimized $Li_3Fe_2(PO_4)_3$ sample was used as cathode material for construction of lithium-ion batteries. All cathodes and anodes were prepared as Section 2.3.3. Three batteries were selected to determine their discharge capacities. For this purpose, they were fully charged by 10 mA constant current for 1 h. After 1 min relaxation, they were discharged by 10 mA constant current. Fig. 14 shows the time–voltage curves of these batteries during 3 consecutive discharge processes. Based on these curves, discharge capacities, mid point voltage (MPV) and power densities were calculated. It should be mentioned that the 3rd battery was used for 6 consecutive charge and discharge exams, but only first 3 discharge curves were shown in Fig. 14. The obtained results were summarized in Table 4. As the data shows, discharge capacity is increased from 122.0 mAh g^{-1} to 128.0 mAh g^{-1} during the first

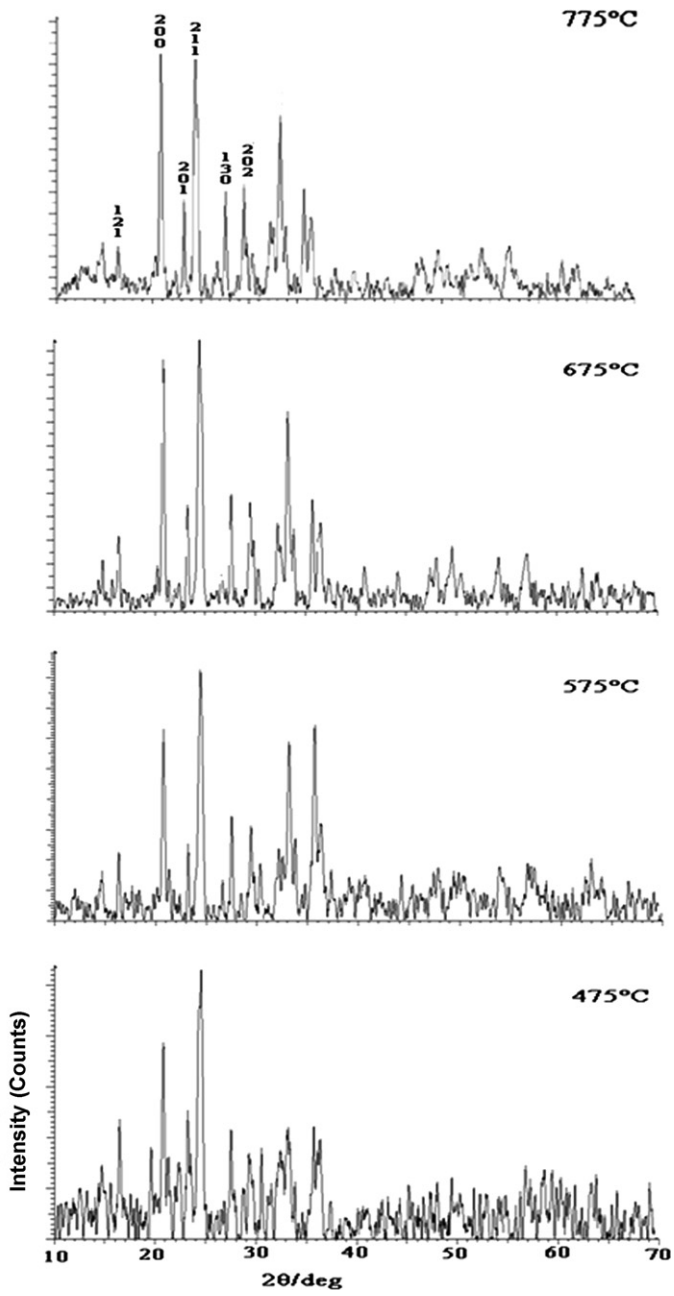

Fig. 8. XRD patterns of the samples synthesized at different temperatures.

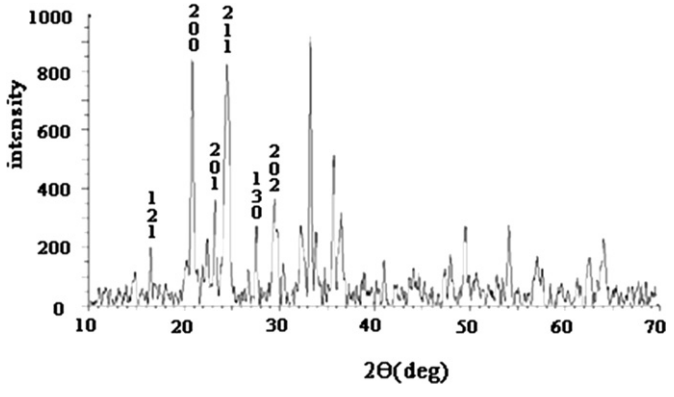

Fig. 9. XRD patterns of the sample synthesized under N_2 atmosphere.

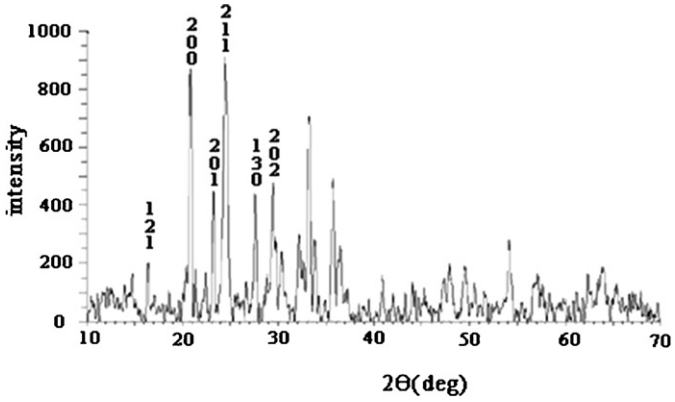

Fig. 10. XRD patterns of the sample synthesized under H_2/N_2 (10/90) atmosphere.

Table 4
Results of consecutive discharge tests by constant current method for 3 constructed batteries.

Battery no.	Discharge no.	MPV (V)	Capacity ($mAh\,g^{-1}$)	Power density ($mW\,g^{-1}$)
1	1	2.7	122.6	331.0
	2	3.1	124.5	386.0
	3	3.1	127.0	393.4
2	1	3.1	122.0	378.1
	2	3.2	126.0	403.4
	3	3.2	128.0	409.6
3	1	3.1	123.2	382.1
	2	3.1	124.5	386.0
	3	3.2	126.9	406.0
	4	3.2	127.0	406.4
	5	3.2	126.8	405.9
	6	3.2	127.0	406.4
Average		3.1	125.5	391.3

3 cycles. As it was mentioned in the CV results, this concept can be explained by converting of Fe_2O_3 and Li_3PO_4 impurities into $Li_3Fe_2(PO_4)_3$. The presented data in Table 4 shows the synthesized material is a suitable selection as cathode of lithium-ion batteries. The obtained capacities are better than all previous reports [28,29,41,44,52,61].

For evaluation cycle life of the constructed batteries, one battery was charged and then discharged for 75 consecutive cycles. Each cycle included a charge by 10 mA constant current for 1 h, 1 min rest and discharge by 10 mA constant current to reach cut off voltage of 2.3 V. The discharge capacity for each cycle was determined and the obtained results are shown in Fig. 15. The obtained results show that the battery capacity is increased from cycle 1 to 3. These results confirmed the results of CV studies. After cycle 3, battery discharge capacity is approximately constant up to cycle 50 and then, the battery capacity is decreased up to 5% at cycle 75. These results confirm that the synthesized nanoparticles are suitable material for using as cathode material in lithium-ion batteries and they have high discharge capacity and long cycle life.

Morcrette et al. [44] observed reversible capacities as high as $110\,mAh\,g^{-1}$ at C/20 regime with an excellent capacity retention. Sato et al. [52] reported, $Li_3Fe_2(PO_4)_3$ delivers a good cycle performance, about 85% capacity efficiency after 10 cycles with a discharge capacity more than $80\,mAh\,g^{-1}$ under a relatively large current density of $0.5\,mA\,cm^{-2}$.

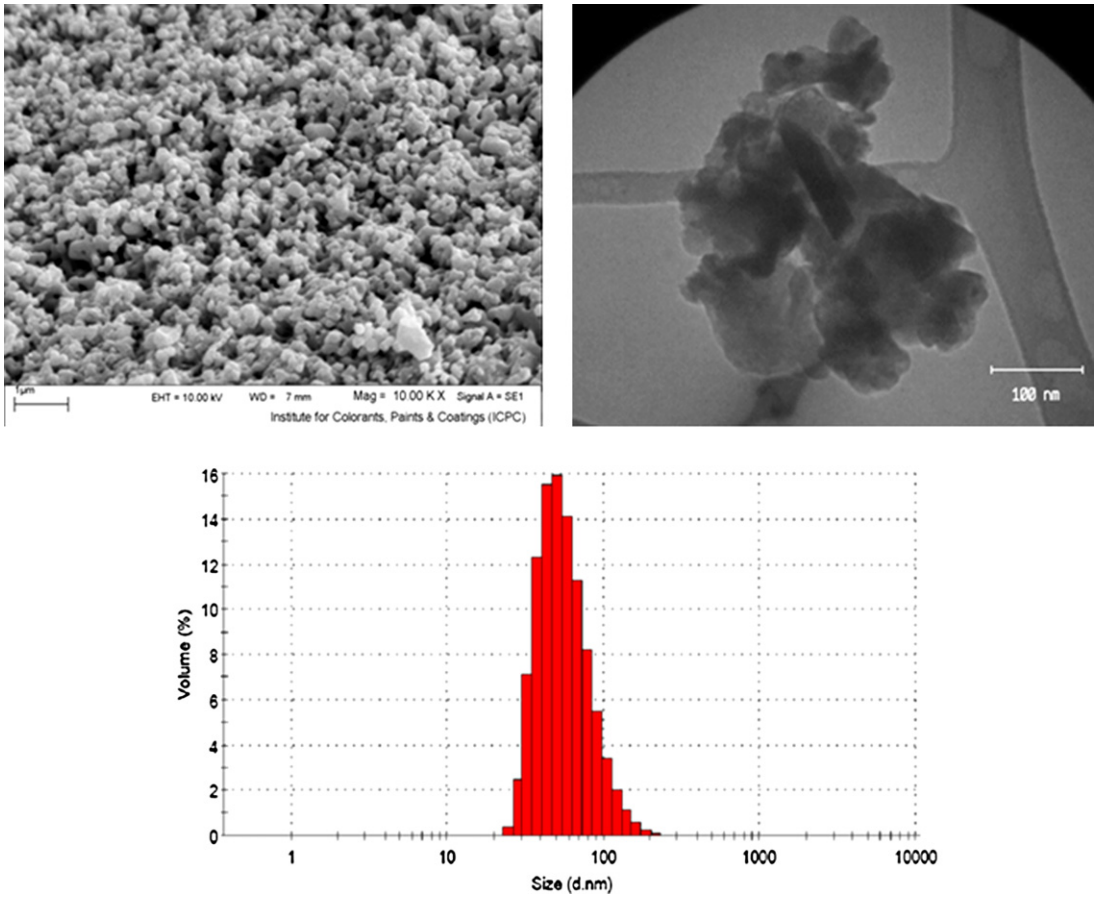

Fig. 11. SEM and TEM images and particle sizes distribution diagram for the optimized sample.

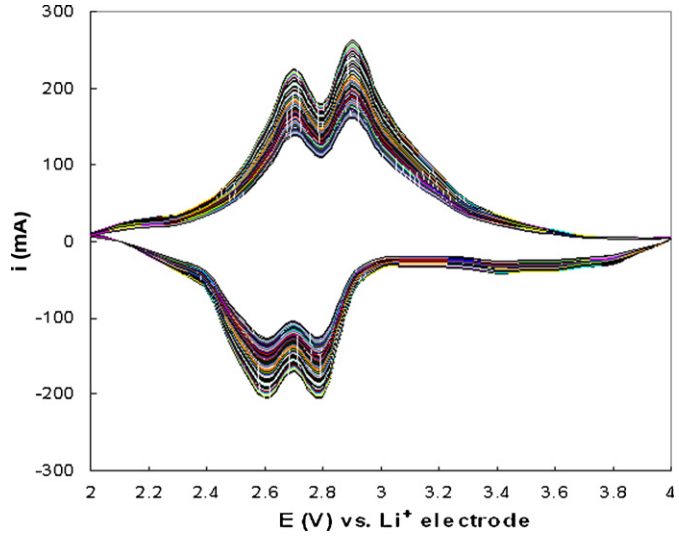

Fig. 12. Fifty consecutive cyclic voltammograms of the synthesized $Li_3Fe_2(PO_4)_3$ sample in the electrolyte including 1 M $LiPF_6$ solution in 1:1 EC and DMC as mixed solvent under Argon atmosphere vs. two lithium electrodes as counter and reference electrodes.

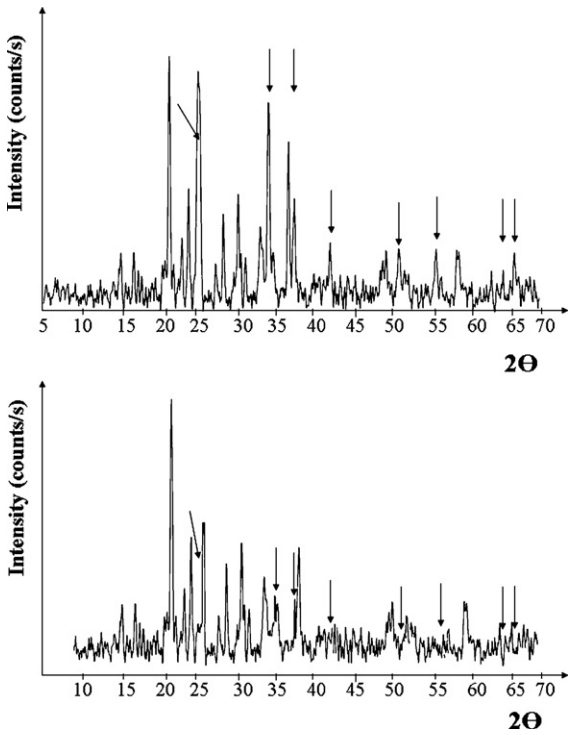

Fig. 13. XRD patterns for the dried paste of working electrode which used in CV studies before (top image) and after 50 cycles CV experiments (down image).

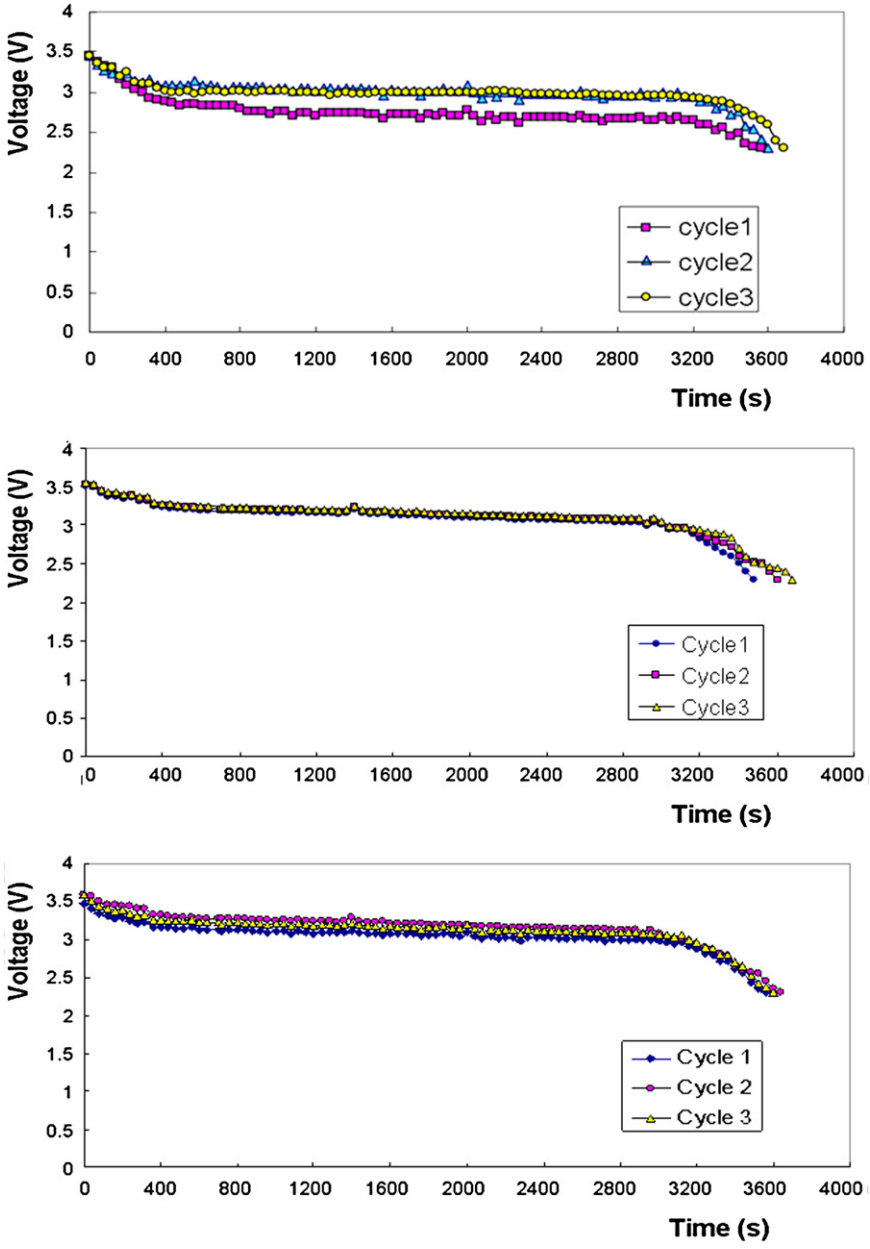

Fig. 14. Discharge curves of 3 constructed batteries during 3 consecutive discharges.

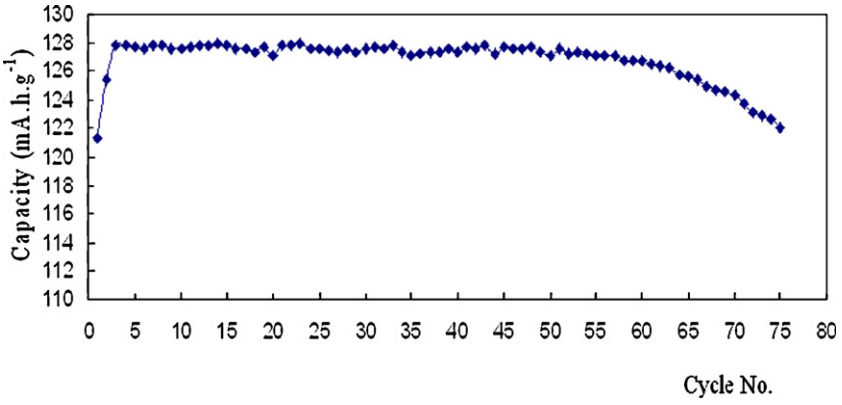

Fig. 15. Variation of discharge capacity during 75 consecutive discharge cycles.

4. Conclusions

Based on the obtained experimental results in this work, the sol–gel combustion method based on PVA as gel making agent can be used as a powerful method to synthesize $Li_3Fe_2(PO_4)_3$ nanoparticles. In this procedure, $Li_3Fe_2(PO_4)_3$ is synthesized in nanometer scale which expected it has some improved discharge capacity and life cycle as the cathode of lithium-ion batteries. The synthesized method used in this work has advantages of low cost of raw material, simple process and short synthesis time. Cyclic voltammetry studies showed that the prepared nanoparticles have good reversible redox reactions. The impurities of the sample are converted into electroactive material and cause to increase both the redox currents and discharge capacity of lithium-ion batteries during some first cycles. The synthesized $Li_3Fe_2(PO_4)_3$ sample showed high discharge capacity (125.5 mAh g^{-1}) and long cycle life.

Acknowledgement

We gratefully acknowledge the support of this work by Abhar Payame Noor University (*PNU*) Research Council.

References

[1] T. Ohzuku, R.J. Brodd, J. Power Sources 174 (2007) 449.
[2] H. Bih, L. Bih, B. Manoun, M. Azdouz, S. Benmokhtar, P. Lazor, J. Mol. Struct. 936 (2009) 147.
[3] J. Vetter, P. Novak, M.R. Wagner, C. Veit, K.-C. Moller, J.O. Besenhard, M. Winter, M. Wohlfahrt-Mehrens, C. Vogler, A. Hammouche, J. Power Sources 147 (2005) 269.
[4] T. Ohzuku, A. Ueda, M. Nagayama, Y. Iwakoshi, H. Komori, Electrochim. Acta 38 (1993) 1159.
[5] P. Kalyani, N. Kalaiselvi, N.G. Renganathan, M. Raghavan, Mater. Res. Bull. 39 (2004) 41.
[6] R.V. Moshtev, P. Zatilova, V. Manew, A. Sato, J. Power Sources 54 (1995) 329.
[7] Y. Nitta, K. Okamura, K. Haraguchi, S. Kobayashi, A. Ohta, J. Power Sources 54 (1995) 511.
[8] R. Kanno, H. Kubo, Y. Kawamoto, T. Kamiyama, F. Izumi, Y. Takeda, M. Takano, J. Solid State Chem. 110 (1994) 216.
[9] D.D. MacNeil, Z. Lu, Z. Chen, J.R. Dahn, J. Power Sources 108 (2002) 8.
[10] M. Takahashi, S.I. Tobishima, K. Takei, Y. Sakurai, Solid State Ionics 148 (2002) 283.
[11] M.S. Whittingham, Chem. Rev. 104 (2004) 4271.
[12] E. Rossen, J.N. Reimers, J.R. Dahn, Solid State Ionics 62 (1993) 53.
[13] J. Cho, B. Park, Lithium Battery Disscussion Electrode Materials, Bordeaux, Abstract 1 (2003).
[14] Z. Chen, J.R. Dahn, Electrochim. Acta 49 (2004) 1079.
[15] S. Levasseur, M. Menetrier, E. Suard, C. Delmas, Solid State Ionics 128 (2000) 11.
[16] N. Imanishi, M. Fujiyoshi, Y. Takeda, Y. Yamamoto, M. Tabuchi, Solid State Ionics 118 (1999) 121.
[17] A. Manthiram, J.B. Goodenough, J. Solid State Chem. 71 (1987) 349.
[18] G. Amatucci, J.M. Tarascon, J. Electrochem. Soc. 149K (2002) 31.
[19] L. He, Sh. Tang, Zh. Chen, H. Du, Solar Energy Mater. Solar Cells 62 (2000) 117.
[20] T. Ohzuku, M. Kitagawa, T. Hirai, J. Electrochem. Soc. 137 (1990) 769.
[21] D. Peramonage, K.M. Abraham, J. Electrochem. Soc. 145 (1998) 1131.
[22] Y. Xia, H. Takeshige, H. Noguchi, M. Yoshio, J. Power Sources 56 (1995) 61.
[23] J.C. Hunter, J. Solid State Chem. 39 (1991) 2859.
[24] Z. Lu, D.D. MacNeil, J.R. Dahn, Electrochem. Solid State Lett. 4 (2001) A191.
[25] M.M. Deoff, T.J. Richardson, L.J. Kepley, Electrochem. Soc. 143 (1996) 2507.
[26] S. Okada, K.S. Nanjundaswamy, A. Manthiram, J.B. Goodenough, H. Ohtsuka, H. Arai, J. Yamaki, 36th Power Sources Conference, June 6–9, 1994.
[27] A.K. Padhi, K.S. Nanjundaswamy, J.B. Goodenough, J. Electrochem. Soc. 144 (1997) 1188.
[28] C. Masquelier, A.K. Padhi, K.S. Nanjundaswamy, J.B. Goodenough, J. Solid State Chem. 135 (1998) 228.
[29] A.K. Padhi, K.S. Nanjundaswamy, C. Masquelier, S. Okada, J.B. Goodenough, J. Electrochem. Soc. 144 (1997) 1609.
[30] D. Jugovi, D. Uskokovi, J. Power Sources 190 (2009) 538.
[31] D. Morgan, G. Ceder, M.Y. Saidi, J. Barker, J. Swoyer, H. Huang, G. Adamson, Chem. Mater. 14 (2002) 4684.
[32] J. Chen, M.J. Vacchio, Sh. Wang, N. Chernova, P.Y. Zavalij, M.S. Whittingham, Solid State Ionics 178 (2008) 1676.
[33] A.K. Padhi, K.S. Nanjundaswamy, C. Masquelier, J.B. Goodenough, J. Electrochem. Soc. 144 (8) (1997) 2581.
[34] C. Wurm, M. Morcrette, G. Rousse, L. Dupont, C. Masquelier, Chem. Mater. 14 (2002) 2701.
[35] C. Delacourt, P. Poizot, J.M. Tarascon, C. Masquelier, Nat. Mater. 4 (2005) 254.
[36] C. Masquelier, C. Wurm, J. Rodriguez-Carvajal, J. Gaubicher, L. Nazar, Chem. Mater. 12 (2) (2000) 525.
[37] F. d'Yvoire, M. Pintard-Scrépel, E. Bretey, M. De la Rochère, Solid State Ionics 10 (1983) 851.
[38] A.B. Bykov, A.P. Chirkin, L.N. Demyanets, S.N. Doronin, E.A. Genkina, A.K. Ivanov-Shits, I.P. KOndratyuk, B.A. Maksimov, O.K. Melnikov, L.N. Muradyan, V.I. Simov, V.A. Timofeeva, Solid State Ionics 38 (1990) 31.
[39] K.S. Nanjundaswamy, A.K. Padhi, J.B. Goodenough, S. Okada, H. Ohtsuka, H. Arai, J. Yamaki, Solid State Ionics 92 (1996) 1.
[40] A.K. Ivanov-Schitz, A.V. Nistuk, N.G. Chaban, Solid State Ionics 139 (2001) 153.
[41] A.S. Andersson, B. Kalska, P. Eyob, D. Aernout, L. Häggstrom, J.O. Thomas, Solid State Ionics 140 (2001) 63.
[42] J.K. Sun, F.Q. Huang, Y.M. Wang, Z.C. Shan, Z.Q. Liu, M.L. Liu, Y.J. Xia, K.Q. Li, J. Alloys Compd. 469 (2009) 327.
[43] K. Nagamine, K. Hirose, T. Honma, T. Komatsu, Solid State Ionics 179 (2008) 508–515.
[44] M. Morcrette, C. Wurm, Ch. Masquelier, Solid State Sci. 4 (2002) 239.
[45] A.S. Andersson, J.O. Thomas, J. Power Sources 97–98 (2001) 498.
[46] A.S. Andersson, J.O. Thomas, B. Kalska, L. Haggstrom, Electrochem. Solid-State Lett. 3 (2000) 66.
[47] S.Y. Chung, J.T. Bloking, Y.M. Chiang, Nat. Mater. 1 (2002) 123.
[48] P.S. Herle, B. Ellis, N. Coombs, L. Nazar, Nat. Mater. 3 (2004) 147.
[49] A. Yamada, H. Koizumi, S.I. Nishimura, N. Sonoyama, R. Kanno, M. Yonemura, T. Nakamura, Y. Kobayashi, Nat. Mater. 5 (2006) 357.
[50] C.H. Mi, Y.X. Cao, X.G. Zhang, X.B. Zhao, H.L. Li, Powder Technol. 181 (2008) 301.
[51] M. Pintard-Screpel, F. D'Yvoire, E. Bretey, Solid State Chem. 3 (1983) 215.
[52] M. Sato, S. Tajimi, H. Okawa, K. Uematsu, K. Toda, Solid State Ionics 152–153 (2002) 247.
[53] G. Butt, N. Sammes, G. Tompsett, A. Smirnova, O. Yamamoto, J. Power Sources 134 (2004) 72.
[54] Sh. Yang, P.Y. Zavalij, M. Stanley, Whittingham, Electrochem. Commun. 3 (2001) 505.
[55] A. Ait Salah, P. Jozwiak, J. Garbarczyk, K. Benkhouja, K. Zaghib, F. Gendron, C.M. Julien, J. Power Sources 140 (2005) 370.
[56] A. Ait Salah, P. Jozwiak, K. Zaghib, J. Garbarczyk, F. Gendron, A. Maugerd, C.M. Julien, Spectrochim. Acta A 65 (2006) 1007.
[57] K. Hirose, T. Honma, Y. Benino, T. Komatsu, Solid State Ionics 178 (2007) 801.
[58] H. Karami, O. Rostami-Ostadkalayeh, J. Clust. Sci. 20 (2009) 587.
[59] S.J. Gregg, K.S.W. Sing, Adsorption, Surface Area and Porosity, Academic Press, London, 1967.
[60] E.P. Barrett, L.G. Joyner, P.P. Halenda, J. Chem. Soc. 73 (1951) 373.
[61] S. Patoux, C. Wurm, M. Morcrette, G. Rousse, Ch. Masquelier, J. Power Sources 119–121 (2003) 278.